

Design and morphological investigation of high-χ catechol-containing styrenic block copolymers

Guillaume Pino, Cian Cummins, Daniele Mantione, Nils Demazy, Alberto Alvarez- Fernandez, Stefan Guldin, Guillaume Fleury, Georges Hadziioannou, Eric Cloutet, Cyril Brochon

▶ **To cite this version:**

Guillaume Pino, Cian Cummins, Daniele Mantione, Nils Demazy, Alberto Alvarez- Fernandez, et al.. Design and morphological investigation of high-χ catechol-containing styrenic block copolymers. Macromolecules, In press, 10.1021/acs.macromol.2c00476 . hal-03728252

HAL Id: hal-03728252
https://hal.science/hal-03728252

Submitted on 20 Jul 2022

HAL is a multi-disciplinary open access archive for the deposit and dissemination of scientific research documents, whether they are published or not. The documents may come from teaching and research institutions in France or abroad, or from public or private research centers.

L'archive ouverte pluridisciplinaire **HAL**, est destinée au dépôt et à la diffusion de documents scientifiques de niveau recherche, publiés ou non, émanant des établissements d'enseignement et de recherche français ou étrangers, des laboratoires publics ou privés.

Design and morphological investigation of high-χ catechol-containing styrenic block copolymers

Guillaume Pino,[1] Cian Cummins,[1] Daniele Mantione,[3] Nils Demazy,[1] Alberto Alvarez-Fernandez,[2] Stefan Guldin,[2] Guillaume Fleury,[1,*] Georges Hadziioannou,[1] Eric Cloutet,[1] Cyril Brochon[1,*]

[1] Univ. Bordeaux, CNRS, Bordeaux INP, LCPO, UMR 5629, F-33600, Pessac, France

[2] Department of Chemical Engineering, University College London, Torrington Place, London, UK

[3] POLYKEY Polymers, Joxe Mari Korta Center, Avda. Tolosa 72, 20018 Donostia-San Sebastian, Spain.

Guillaume Fleury: gfleury@enscbp.fr

Cyril Brochon: cyril.brochon@enscbp.fr

ABSTRACT:

We report the synthesis of multifunctional block copolymers (BCPs) showing a high Flory-Huggins interaction parameter (χ) which enable sub-10 nm line space structures for a low degree of polymerization (N). The high χ BCPs are based on a poly(3,4-dihydroxystyrene)-*block*-poly(4-trimethylsilylstyrene) (PDHS-*b*-PTMSS) architecture. The controlled synthesis of the PDHS-*b*-PTMSS precursors was performed using user-friendly sequential nitroxide mediated polymerization (NMP) polymerization of 3,4-diacetoxysytrene and 4-trimethylsilylstyrene (PDAS-*b*-PTMSS). Thereafter, acid-catalyzed deprotection of the acetoxy moieties produced a library of PDHS-*b*-PTMSS BCPs with molecular weights ranging from

2.1 to 44.5 kg/mol. Bulk lamellar and cylindrical structures with periodicities as small as 8 nm were revealed by small-angle X-ray scattering. Moreover, PDHS-*b*-PTMSS thin films were assembled using solvent vapor annealing to define 10 nm line-space patterns in favorable conditions, i.e. at 20°C for 20 minutes. In summary, our work brings further knowledge to the BCP toolbox for next-generation nano-manufacturing needs.

INTRODUCTION:

Block copolymers (BCPs) can self-assemble into various morphologies including spheres, cylinders, gyroid and lamellae.[1] Such periodic structures with nanometric periodicity can subsequently be used in diverse applications including ultrafiltration membranes,[2] batteries[3], and photonics[4,5]. Additionally, the microphase separation of BCP in thin films has also been investigated for the generation of etch masks for next-generation semiconductor patterning.[6,7] Their unique ability to form discrete structures offers a bottom-up complementary methodology to alleviate photolithography issues including cost, throughput and size limitations. The minimum possible pitch size (L_0) is linked to the overall BCP degree of polymerization (N) and the Flory-Huggins interaction parameter (χ), while the morphology is governed by the volume fraction (*f*) of each block. In the case of symmetric di-BCP architectures, lamellar structures are obtained which can be subsequently used to form line-space patterns in a thin film configuration. Lamellar structures have been the focus of intensive research activities for advanced pattern transfer lithography in electronics manufacturing.[8,9] Nevertheless, cylindrical BCP systems for the definition of line-space features have recently received a renewed interest as interface effects can be more easily controlled.[10,11] To further reduce BCP periodicity, high χ - low N systems have been targeted through precise macromolecular engineering of BCP systems,[6] with a straightforward strategy consisting in the formation of BCP architecture with highly dissimilar chemical blocks. However, the high dissimilarity in block chemistry leads to large surface energy differences between the BCP domains and is, therefore, an issue for thin-film processing, *e.g.* surface dewetting and controlled orientation of the BCP structures. Moreover, monomers with such contrasting chemistry do not always share the same polymerization pathway. For example, nitroxide mediated polymerization (NMP) of (meth)acrylates monomers, a commonly studied block,[12,13] is still very challenging.[14] Likewise, reversible addition−fragmentation chain-transfer polymerization (RAFT) agents have to be

chosen wisely to give the desired BCP architecture.[15] A pertinent example is poly(styrene)-*block*-poly(lactic acid) (PS-*b*-PLA) which first requires the synthesis of a hydroxy-terminated polystyrene in order to initiate the ring opening polymerization (ROP) of lactide.[16]

A plethora of different monomers have been explored for nanolithography[17] in order to bypass the limited resolution of PS-*b*-PMMA inherent to its low χ value (χ = 0.03 at 150°C).[18] In particular, the use of post-polymerization chemical modifications of PS-*b*-PMMA systems has led to a higher segregation strength. For example, partial hydrogenation of PS-*b*-PMMA was used to produce poly(cyclohexylethylene)-*b*-poly(methyl methacrylate) yielding feature sizes as small as 7.5 nm.[19] More recently, Zhang *et al.*[13] reduced the PMMA block in PS-*b*-PMMA to form an analogue to poly(vinyl alcohol), *i.e.* poly(hydroxyisobutylene). This hydroxy-containing BCP showed a χ value ten times higher than PS-*b*-PMMA. Another prominent strategy to increase a χ value focused on the incorporation of oxygen atoms in one block with PS-*b*-PEO as a representative example.[20–22] Gopalan and co-workers[23] have focused their efforts on the use of poly(4-hydroxystyrene) (P4HS) based BCPs. Their work on P4HS-*b*-PS led to a lamellar microdomain size of 11.8 nm when associated with styrene and produced cylindrical domain sizes of 11.5 nm with poly(*tert*-butylstyrene). Polymerization of the tetrahydropyranyloxy-protected precursors was first processed, and then its acid-catalyzed deprotection led to the desired hydroxy-styrene. Following this work and stating that adding additional oxygen atoms to the BCP architecture should lead to higher hydrophilic properties, Kwak *et al.*[24] introduced a catechol-containing polystyrene *i.e.*, namely poly(3,4-dihydroxystyrene) (PDHS). PDHS was made by deprotection of poly(dimethoxystyrene) using BBr_3 as a Lewis acid. Temperature-dependent SAXS measurements on PDHS-*b*-PS demonstrated an interestingly high χ value of 0.7 at 170°C.

On the other hand, the incorporation of silicon atoms often leads to an accentuated hydrophobic behavior while robust etch masks can be developed given the propensity of silicon-containing

blocks to form SiO_x. As a consequence, poly(dimethylsiloxane) (PDMS) is one of the most studied Si-containing blocks for BCP nano-manufacturing.[25–30] For example Ross and coworkers[31] assembled a P2VP-*b*-PDMS copolymer showing a 6 nm line width with low defectivity and highlighting as well the ability to form a SiO_x hard mask using a CF_4 reactive ion etching (RIE). Gopalan and co-workers reported the use of a poly(3-hydroxystyrene)-*b*-PDMS in order to obtain both a high χ value and etch contrast. Accordingly, they reported a χ value of 0.39 at 150°C which enabled the formation of a well-ordered 7.5 nm pitch lamellar structure and an etch selectivity of 15:1 facing oxygen RIE. Durand *et al.* worked with silylated styrene derivatives and demonstrated the formation of SiO_x hard mask using poly(4-trimethylsilylstyrene) PTMSS.[32] While the fully hydrophobic PTMSS-*b*-PS showed a moderate interaction parameter of 0.047 at 150°C, the substitution of the PS block by the more hydrophilic poly(4-methoxystyrene) block led to a higher χ value of 0.14 at 150°C.

This work reports the controlled synthesis of a novel BCP set consisting of PDHS-*b*-PTMSS. PDHS has demonstrated important hydrophilic properties and can yield a high interaction parameter when linked to a hydrophobic block thus leading to self-assembly at low N. In order to access catechol styrene repeating unit, poly(diacetoxystyrene) (PDAS) was chosen as a precursor for its ease to lose the protecting diacetoxy moieties in mild acid-catalyzed conditions. Interestingly, 3,4-diacetoxystyene monomer could be prepared from a bio-based precursor, caffeic acid. The polymerization was conducted using NMP which is less sensitive than anionic polymerization and more versatile in the monomer sequence. Furthermore, NMP exhibits a good efficiency for styrene-based monomers polymerization and without any byproducts. A good control (controlled M_n and narrow molecular weight distribution) and a high conversion of styrenic monomers were observed using N-*tert*-butyl-1-diethylphosphono-2,2-dimethylpropyl nitroxide (SG_1 alkoxyamine) controller. SAXS analysis in bulk demonstrated the ability of this system to resolve lamellar and cylindrical morphologies with a pitch as small

as 8 nm. Self-assembled structures with feature sizes as small as 6 nm were also observed in thin-film configuration using solvent vapors as annealing treatment. This work also highlights the potential of this BCP system to generate ordered double oxide patterns using the strong affinity of catechol moieties with metal ions and the propensity of the silylated styrene derivatives to form SiO_x through RIE.

EXPERIMENTAL:

Materials. Deuterated solvent and NMR tubes were purchased from Eurisotop. N-tert-butyl-1-diethylphosphono-2,2-dimethylpropyl nitroxide, (SG_1 alkoxyamine) was kindly provided by Arkema. Caffeic acid was purchased from TCI and 3,4-diacetoxystyrene was synthesized as reported elsewhere (see Supporting Information section 2 and Figure S1-2 for details).[33] Trimethyl silylstyrene was synthesized from bromostyrene following the procedure reported by Lee *et al*.[34] Solvents used for solvent vapor annealing were purchased from Sigma Aldrich and were used as received. All other chemicals and solvents were supplied from Fisher Scientific and used without further purification.

Synthesis of poly(3,4-diacetoxystyrene) (PDAS-SG_1): In a flame dried Schlenk, 1 g of 3,4-diacetoxystyrene was mixed with 76.6 mg of SG_1-blocbuilder and 0.4 ml of DMF. The Schlenk was allowed to stir for 10 min to obtain a homogeneous mixture. Three freeze-pump-thaw cycles were then performed to remove all oxygen traces. The polymerization was then started by putting the argon-filled Schlenk in a 120 °C preheated oil bath. After 3 hours, the vessel was put in liquid nitrogen to stop the polymerization and the viscous mixture was diluted with THF before precipitation in cyclohexane, using 100 ml for each gram of monomer. The density of PDAS at 25°C was estimated using a pycnometer at 1.2 $g.cm^{-3}$.

Synthesis of poly(3,4-diacetoxystyrene)-*b*-poly(4-trimethylsilylstyrene): In a flame dried Schlenk, 0.5 g of PDAS-SG_1, 2 g of TMSS and 4 ml of DMF were added. Then 33 µL (0.05 eq) of 1M SG_1 nitroxide radical solution in DMF was added. After complete dissolution, the Schlenk was placed at 120 °C for 2 hours. The crude mixture was diluted in THF before precipitation in ≈ 100 ml of water/methanol [70/30], the obtained white powder was then filtered with a fritted glass. The purification through precipitation was repeated twice to remove all traces of residual monomer, using the minimum amount of THF to re-dissolve the polymer. The obtained white powder was finally dried in a vacuum oven at 60 °C for 24 hours.

Hydrolysis of PTMSS-*b*-PDAS: PDAS block was deprotected in acidic conditions by dissolving the BCP in THF (2 ml/g). Then 0.2 ml/g of HCl in water (10M) was added and left stirring at 50 °C for 15 hours. The polymer was then precipitated in water and filtered. The obtained reddish powder was dried under vacuum.

Thin-film self-assembly: Silicon substrates, with a native silicon dioxide layer (≈ 2 nm), were diced into 1 x 1 cm^2 pieces and ultra-sonicated in n-butyl acetate for 10 minutes. Prior to deposition, substrates were blown dry with N2. 1 wt. % PDHS-*b*-PTMSS solutions in n-butylacetate were deposited upon the wafers at 3000 rpm for 30 seconds. The BCP layers after spin-coating were uniform (root mean square roughness ≈ 0.6 nm) as demonstrated by large-sized AFM height images shown in Figure S8. The BCP films were subsequently exposed to a 1:1 THF-toluene mixture of solvent vapors in 50 cm3 glass jars for an optimized time of 20 minutes to promote self-assembly at room temperature. These static SVA conditions yielded stable BCP layers with respect to dewetting as demonstrated by the large-sized AFM height images provided in Figure S9. Homopolymer thin film surface energies were characterized by goniometry using a Kruss drop shape analyzer DSA100 in sessile drop mode.

Nuclear magnetic resonance (NMR): NMR spectra were all recorded at ambient temperature using a liquid-state 400 MHz NMR spectrometer (Bruker AVANCE I) with a 5 mm BBFO probe in the appropriate deuterated solvent. Data are reported in chemical shift (ppm), multiplicity (s, singlet; d, doublet; t, triplet; dd, double doublet; q, quartet); the signals are referenced to the residual solvent THF-d_6 (δ = 1.72, 3.58 ppm ^1H, 39.520 ppm ^{13}C); $CDCl_3$ (δ = 7.26 ppm ^1H, 77.160 ppm ^{13}C).

Size exclusion chromatography (SEC): SEC measurements were performed with a Viscotek TDAmax system from Malvern Instruments that consists of an integrated solvent and sample delivery module (GPCmax) and a Tetra Detector Array (TDA). THF was used as the mobile phase at a flow rate of 0.8 mL/min and TCB as a flow rate marker. All polymers were injected

at a concentration of 5 mg/mL (100 µL of solution) after filtration through a 0.45 µm pore-size membrane. The separation was carried out on two Agilent columns [2 × PLgel 5 µm Mixed C (300 × 7.5 mm)] and a guard column (PL gel 5 µm). Columns and detectors were maintained at 30 °C. Relative molecular weights and dispersity were determined thanks to a conventional calibration obtained with polystyrene narrow standards.

Small-angle X-ray scattering (SAXS). Room temperature SAXS experiments were performed at the Centre de Recherche Paul Pascal (CRPP) at Université de Bordeaux using a high-resolution X-ray spectrometer Xeuss 2.0 from Xenoxs operating with a radiation wavelength of $\lambda = 1.54$ Å. 2D scattering patterns were collected using a PILATUS 300K Dectris detector with a sample-to-detector distance of 1635 mm. The beam center position and the angular range were calibrated using a silver behenate standard sample. The SAXS patterns were radially averaged around the direct beam position using the Xenocs XSACT software. Temperature-dependent SAXS experiments were carried out using a Ganesha 300XL (SAXSLAB) at the EPSRC CNIE research facility service in London (UK) by employing a high brilliance microfocus Cu-source ($\lambda = 1.54$ Å). SAXS patterns were recorded using a Pilatus 300 K solid-state photon-counting detector with a 2 mm beam stop, with a sample-to-detector distance of 950 mm. The beam center and the sample-to-detector distance were calibrated by using the position of diffraction peaks from a standard silver behenate powder. The SAXS patterns were radially averaged around the direct beam position by using the SAXSGUI software.

Thin-film characterization methods. BCP surfaces were characterized using a Dimension FastScan AFM (Bruker) in tapping mode. Silicon cantilevers (Fastscan-A) with a typical tip radius of ≈ 5 nm were used. The resonance frequency of the cantilevers was ≈ 1.4 kHz. A JEOL 7800-E Prime scanning electron microscope (SEM) was used at low voltage acceleration (1 kV) in the super high-resolution gentle beam (GBSH) mode to characterize the oxide nanostructures.

RESULTS AND DISCUSSION:

PDHS-*b*-PTMSS design, synthesis and characterization. Several PDHS-*b*-PTMSS BCPs were synthesized to access lamellar and cylindrical morphologies for the definition of line-space features in thin-film configuration (Scheme 1 and Table 1). This particular block sequence was considered as previous reports have demonstrated that a PDHS block associated with a hydrophobic block (*i.e.* PS) shows one of the highest χ value parameters in literature.[17] The design of the presented BCP system involves the replacement of the PS block with its silicon-containing derivative, *i.e.* PTMSS. The latter leverages the generation of a SiO_x network when subject to oxidant irradiation or plasma etching, thus presenting hard mask properties for potential pattern transfer to an underlying substrate. Such materials are of interest for nanolithography and future semiconductor patterning nodes.[35,36]

Since dihydroxy derivatives act as radical traps during NMP, the strategy used to form PDHS involved a protected precursor. The use of poly(3,4-dimethoxystyrene) as a PDHS precursor is already described in association with demethylating agent BBr_3, a strong and highly reactive Lewis acid.[24] However, in addition to being incompatible with any ether groups-bearing solvents such as THF, BBr_3 might lead to specific $-BBr_2$ / $-Si(Me)_3$ exchange,[37] impeding the use of this deprotection method with a poly(4-trimethylsilylstyrene) block. For these reasons, poly(3,4-diacetoxystyrene) was chosen as a PDHS precursor. The TMSS monomer was synthesized from bromostyrene as already reported by Lee *et al.* through a lithium bromine exchange and addition of chlorotrimethylsilane.[34]

Polymerizations were carried out by NMP using Blocbuilder SG_1 acting both as an initiator and controller. This NMP agent avoids using further radical sources and allows one to reach high conversion (> 70%) with styrenic derivatives while producing polymers with a low dispersity. The addition order was determined as the PDAS macroinitiator showed better reinitiation in respect of PTMSS, and was, thus, polymerized first. The high polarity of PDAS also allowed

easy precipitation in non-polar organic solvents. A kinetic study was performed to verify the living nature of the polymerization. Aliquots were collected at different reaction times and analyzed by ^{1}H-NMR, calculating the number averaged molecular weight ($\overline{M_n}$) by integration of the nitroxide end-chain proton (>N-C**H**(*t*Bu)-). The plot of the number average molecular weight as a function of conversion, presented in Figure S3(a), shows a linear relation, confirming a successfully controlled polymerization.

The SG_1 terminated PDAS homopolymers were purified and analyzed by NMR and SEC prior to their use as macroinitiators for the growth of the PTMSS block. It is noteworthy that during the polymerization of the second block, a catalytic amount of radical controller $SG_1^{\bullet}$ was added to the mixture. This addition is necessary in order to avoid irreversible chain-end reactions occurring at the start of the reaction, thus maintaining good control of the final BCP composition.[38] This control was also confirmed by NMR analysis of the molecular weight evolution, showing a linear dependence with conversion (see Figure S3(b)). Therefore, a series of PDAS-*b*-PTMSS were synthesized and a mild acid-catalyzed deprotection step was performed to yield the desired PDHS-*b*-PTMSS.

Scheme 1. Synthetic scheme for the preparation of PDAS-*b*-PTMSS BCPs *via* NMP

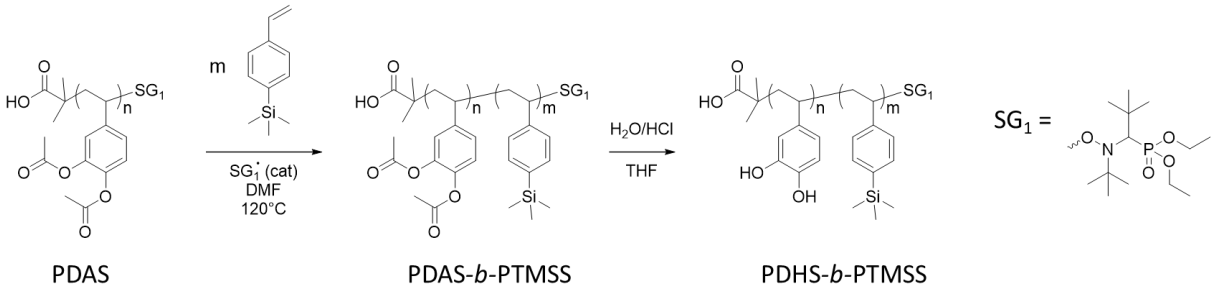


Table 1. Characteristics of PDHS-*b*-PTMSS BCPs.

BCP	$\overline{M}_n$(NMR)[a] kg/mol	$\overline{M}_n$(SEC)[b] kg/mol	Đ[b]	f_{PDHS}[c]	$N_{tot}^{118A^3}$[d]	Morphology[e]	L_0[e] (nm)
PDHS-*b*-PTMSS1	44.5	21	1.6	0.38	609	LAM	50
PDHS-*b*-PTMSS2	34.2	11.9	1.8	0.50	459	LAM	38.2
PDHS-*b*-PTMSS3	15.1	10.4	1.7	0.66	184	CYL	36.5
PDHS-*b*-PTMSS4	16.6	9.4	1.7	0.38	221	LAM	25.1
PDHS-*b*-PTMSS5	8.1	7.2	1.3	0.45	110	LAM	13.6
PDHS-*b*-PTMSS6	5.2	4.8	1.6	0.32	72	CYL	14.3
PDHS-*b*-PTMSS7	4	4	1.4	0.25	57	CYL	11.5
PDHS-*b*-PTMSS8	3.6	2.5	1.4	0.57	46	LAM	8.5
PDHS-*b*-PTMSS9	3.4	4.8	1.2	0.52	45	LAM	8
PDHS-*b*-PTMSS10	2.1	2.3	1.3	0.50	29	DIS	-

[a] Molecular weight calculated with ^{1}H NMR by integration of the >N-C**H**(*t*Bu)- proton of the SG_1 end-chain group at 3.2 ppm. [b] Molecular weight and dispersity (Đ) measured by SEC using PS standards. [c] Volume fraction obtained from ^{1}H NMR by comparing the signals of the acetoxy C(=O)C**H**$_3$ protons (PDAS) with the trimethylsilyl -Si(C**H**$_3$)$_3$ protons (PTMSS). The density of PTMSS (0.96 g/cm^3) and PDHS (1.14 g/cm^3) were taken from Cushen *et al.*[39] and Kwak *et al.*[24], respectively. PDAS density (1.2 g/cm^3) was measured according to Archimedes' principle. [d] Overall degree of polymerization recalculated from NMR data for a reference volume of 118 Å^3 using the aforementioned room temperature densities. [e] Morphology and d-

spacing (L_0) deduced from bulk SAXS analysis using $L_0 = 2\pi/q^*$ for LAM and $L_0 = 4\pi/\sqrt{3}q^*$ for CYL (LAM: lamellar morphology, CYL: Hexagonally packed cylinders).

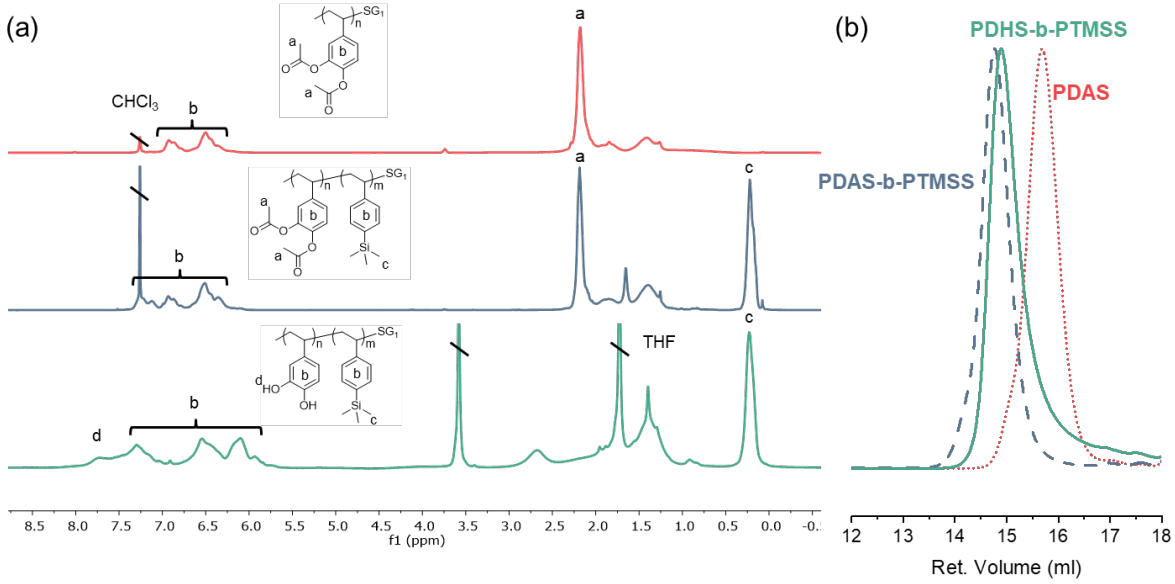


Figure 1. (a) ^{1}H NMR signals recorded for $PDAS_{12}$ and PDAS-*b*-PTMSS6 in $CDCl_3$ and for PDHS-*b*-PTMSS6 in THF-d_8 with the corresponding structures. (b) Normalized SEC overlapped curves: $PDAS_{12}$ (dotted line), PDAS-*b*-PTMSS6 (dashed line) and PDHS-*b*-PTMSS6 (solid line).

Figure 1 (a) shows the ^{1}H NMR spectra of the typical PDAS homopolymer (top spectrum, red), PDAS-*b*-PTMSS (middle spectrum, blue) and PDHS-*b*-PTMSS (bottom spectrum, green). The PDAS ^{1}H NMR spectrum displays the aromatic groups between 6 and 7.5 ppm (signals b) while the methyl groups from the acetoxy moiety appear at 2.2 ppm (signals a). After the growth of the PTMSS block, a new proton signal from the TMS group is apparent at 0.2 ppm (signals c). The deprotection of hydroxyl groups was monitored from the disappearance of the signals at 2.2 ppm concomitant with the appearance of a signal above 7.5 ppm corresponding to the alcohol functions (signal d). The PDAS-*b*-PTMSS spectra presented in Figure S4 were used to

calculate the volume fraction of each block as direct evaluation from the PDHS-*b*-PTMSS spectra is problematic due to signal overlapping between the aromatic moieties of each block and the newly formed alcohol function.

The corresponding SEC traces are displayed in Figure 1 (b). With the growth of PTMSS, the corresponding PDAS-*b*-PTMSS SEC trace (blue dotted curve) shifts to lower retention volume with respect to the PDAS trace (red dashed line). The PDAS-*b*-PTMSS deprotection step induces a shift of the PDHS-*b*-PTMSS SEC trace towards higher volumes (green full line). All the SEC traces for PDAS and PDAS-*b*-PTMSS show narrow dispersity (Đ) (between 1.1 and 1.2), and around 1.5 for the hydroxy-containing PDHS-*b*-PTMSS BCPs (see Figure S5). Since a quantitative deprotection was observed by ^{1}H NMR (further confirmed by FTIR analysis following the C=O stretching band around 1730 cm^{-1} as shown in Figure S6), the increase of dispersity after deprotection is attributed to interactions between the columns and the numerous hydroxy groups in the BCP structure leaving a tail in the SEC signals. DSC measurements further confirmed the deprotection of the acetoxy units. Typical PDAS-*b*-PTMSS heating trace (Figure S7) exhibited two glass transitions at 100 °C and 120 °C for the PDAS and PTMSS blocks, respectively. After deprotection, the glass transition temperature (T_g) of PDAS shifts from 100 °C to 170 °C corresponding to the T_g of PDHS as observed by Nakamura *et al.* on hydroxy-substituted polystyrene.[40] The macromolecular characteristics of the BCPs are summarized in Table 1 (see Table S1 for the macromolecular characteristics of PDAS-*b*-PTMSS intermediates).

Bulk microphase separation. PDHS-*b*-PTMSS BCPs were further analyzed by SAXS to study their microphase separation in the bulk state. All samples were cast from THF and dried under vacuum for 24 hours. Figure 2 displays the SAXS patterns obtained at 25 °C for each PDHS-*b*-PTMSS. The obtained sequence of scattering peaks demonstrates the ability of the PDHS-*b*-PTMSS BCPs to form segregated structures in the bulk with d-spacing as low as 8 nm (see

Table 1). PDHS-*b*-PTMSS1, PDHS-*b*-PTMSS2, PDHS-*b*-PTMSS4, PDHS-*b*-PTMSS5, PDHS-*b*-PTMSS8 and PDHS-*b*-PTMSS9 showed a series of peaks at scattering wavevectors indexed as q/q* = 1:2:3:4 which is consistent with a lamellar mesostructure. In addition, PDHS-*b*-PTMSS3, PDHS-*b*-PTMSS6 and PDHS-*b*-PTMSS7 displayed cylindrical morphologies as confirmed by the q/q* sequence of their respective peaks at 1:√3:√4:√7:√9. The d-spacing was calculated using $L_0 = 2\pi/q^*$ for lamellar structure and $L_0 = 4\pi/\sqrt{3}q^*$ as the cylinder-cylinder distance for the hexagonal morphology.

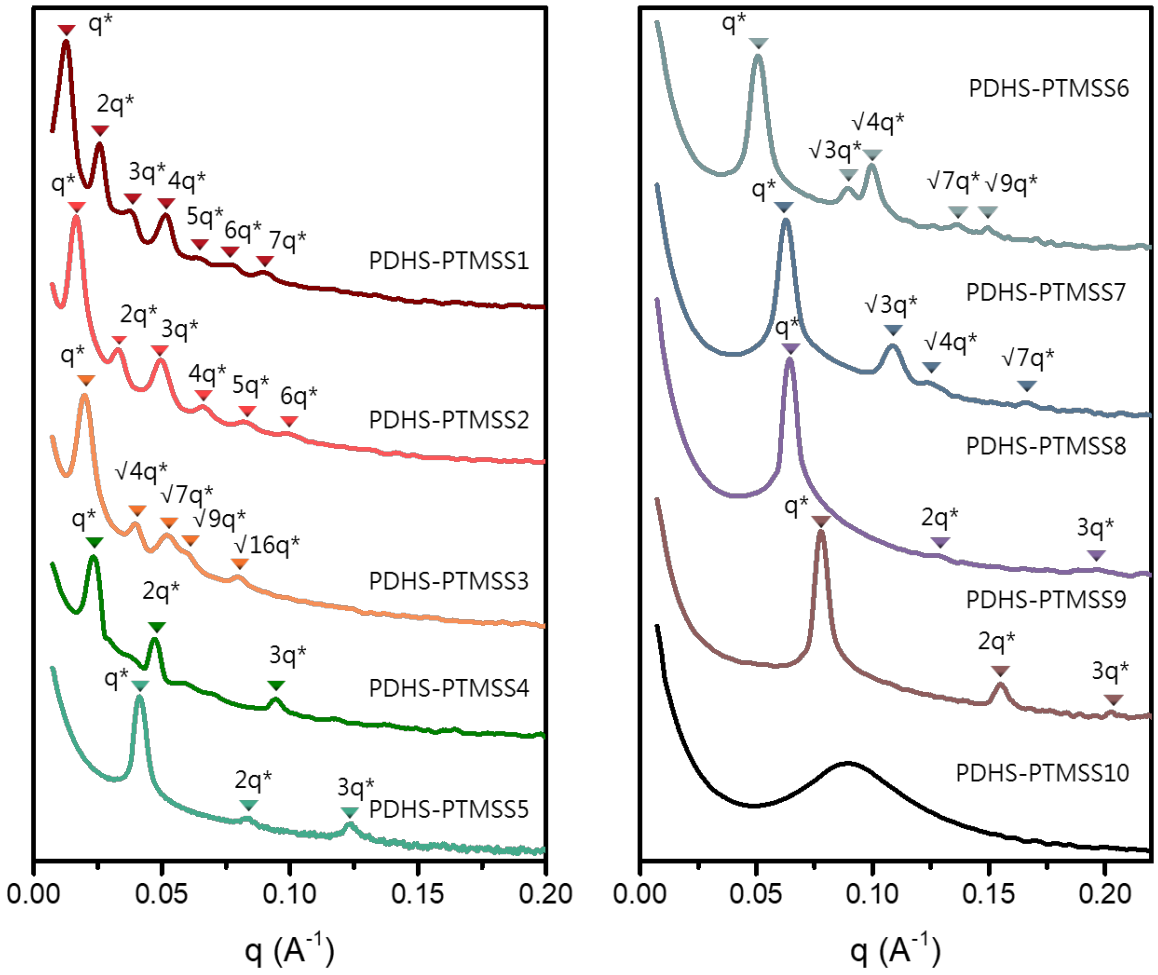


Figure 2. Representative SAXS profiles acquired at 25 °C of all PDHS-*b*-PTMSS BCPs reported in this study. Note that data have been shifted vertically for clarity.

Figure 3 displays the scaling relationship between the BCP d-spacing versus the total degree of polymerization of respective lamellar-forming BCPs based on a 118 Å^3 reference volume. The experimental results show a power law of $L_0 \propto N^{0.68\pm0.03}$ which is consistent with the strong segregation theory prediction *i.e.,* $L_0 \sim N^{2/3}$.[41]

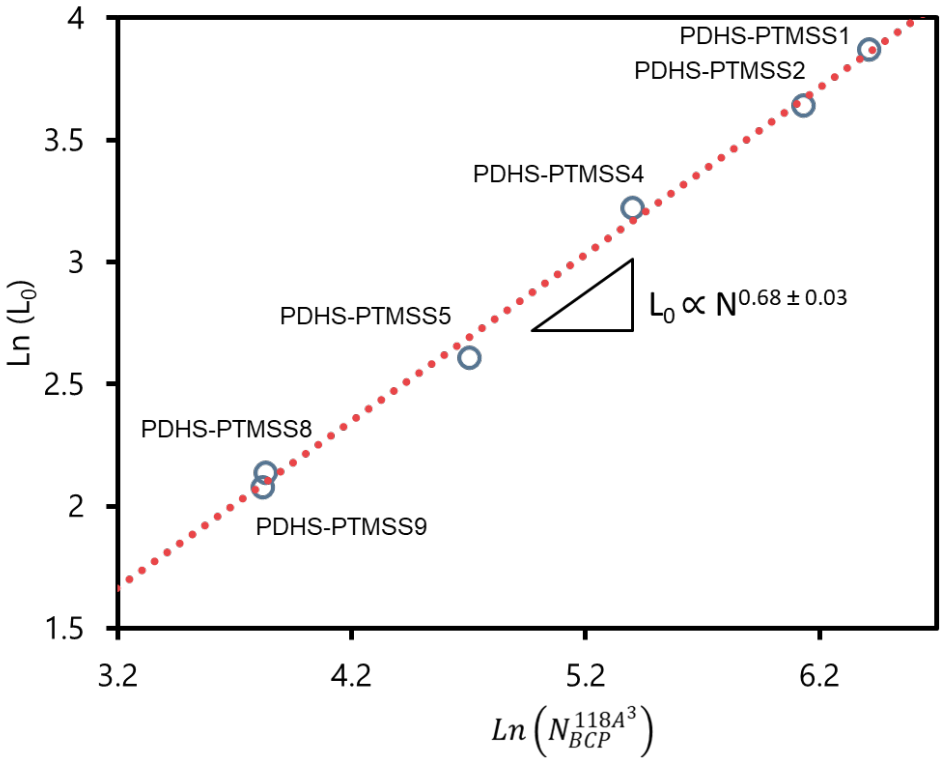


Figure 3. Plot of the scaling relationship of lamellar PDHS-*b*-PTMSS BCPs d-spacing (L_0) with respect to the total degree of polymerization based on 118 Å^3 reference volume.

The Flory-Huggins parameter was subsequently estimated through Leibler's mean-field theory using temperature resolved SAXS.[42] The absolute SAXS intensities were plotted against the scattering vector for the disordered PDHS-*b*-PTMSS10 sample (M_n = 2.1 kg/mol) at temperatures ranging from 160 to 200 °C. A mean-field expression for the segment-segment interaction parameter corrected from the effects of dispersity and segmental volume asymmetry has been extracted from the scattering profile (see Supporting Information Section 3 and Table

S2 for details). The resulting temperature-dependent Flory-Huggins parameter is displayed in Figure 4 and a value of 0.56 at 140 °C was calculated. This value is in the same order of magnitude than other silicon-containing BCPs such as PTMSS-*b*-PLA (0.41 at 140 °C)[43] or PDMS-*b*-PHS (0.39 at 140 °C)[44].

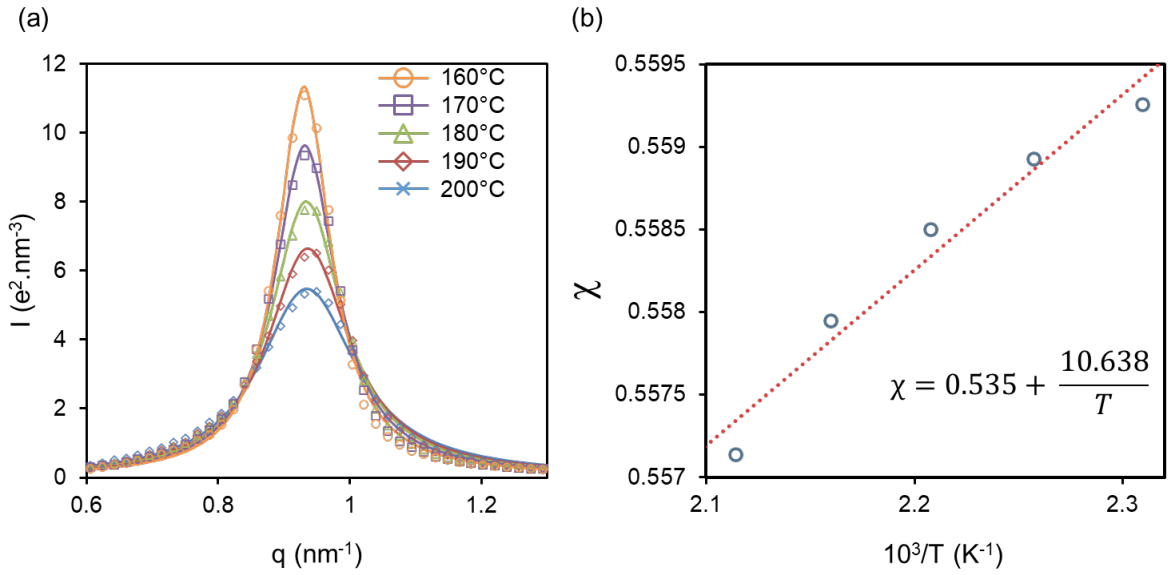


Figure 4. (a) Temperature-resolved SAXS intensity profiles of PDHS-*b*-PTMSS10 fitted using Leibler's mean-field theory at the vicinity of the scattering signal associated with density fluctuations. (b) Dependence of the Flory-Huggins parameter as a function of temperature extracted from the temperature-resolved SAXS intensity profiles.

PDHS-*b*-PTMSS self-assembly in thin films

To highlight the use of the newly designed PDHS-*b*-PTMSS BCPs, we investigated their ability to form thin film patterns. PDHS-*b*-PTMSS BCPs were spin-coated on silicon wafer substrates resulting in film thicknesses of ≈ 15-30 nm. Solvent vapor annealing (SVA) was used to promote self-assembly as previously reported in literature for hydroxystyrene-containing BCPs.[45–47] The use of SVA is also driven by the high T_g of the PDHS block (≈ 160-180 °C)

which limits the chain mobility needed to achieve phase separation via thermal annealing. Moreover, it is known that hydroxystyrene derivatives can cross-link at elevated temperatures and could thus be a problematic treatment method.[48]

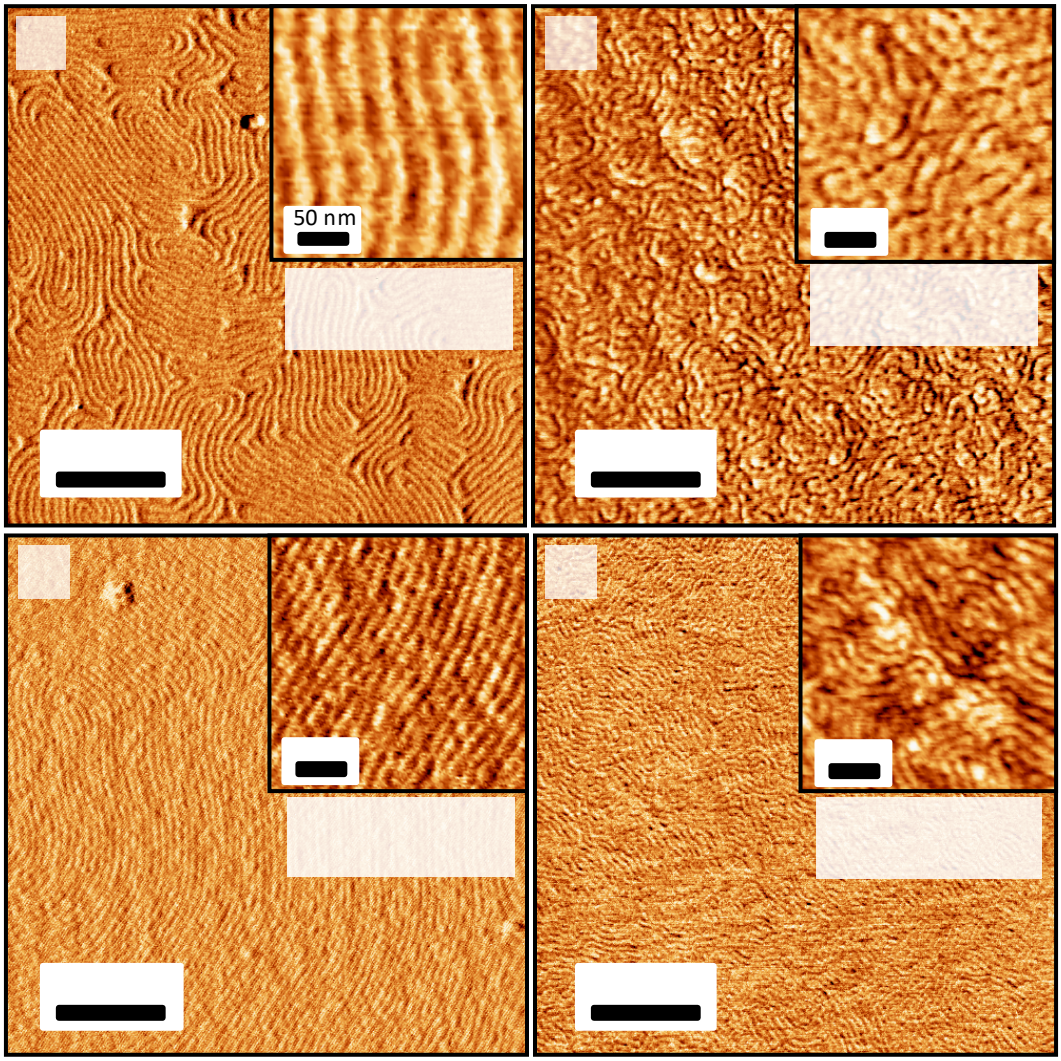


Figure 5. AFM phase images of the self-assembled PDHS-*b*-PTMSS films on silicon surfaces. **(a)** PDHS-*b*-PTMSS4, **(b)** PDHS-*b*-PTMSS5, **(c)** PDHS-*b*-PTMSS6, and **(d)** PDHS-*b*-PTMSS7. PDHS-*b*-PTMSS films were solvent annealed in a THF/toluene mixture atmosphere at RT for 20 min.

Figure 5 a-d displays the AFM phase images of selected PDHS-*b*-PTMSS thin films after 20 minutes SVA with a 1:1 mixture of toluene ($\delta_{Toluene}$ = 18.3 $MPa^{1/2}$) and THF (δ_{THF} = 19.5 $MPa^{1/2}$). The SVA method using a mixture of solvent was chosen in order to limit an asymmetric swelling of the BCP domains which could modify the effective volume fraction due to the large difference in solubility parameters between PDHS (δ_{PDHS} = 24.2 $MPa^{1/2}$) and PTMSS (δ_{PTMSS} = 16.6 $MPa_{1/2}$) [39] (see Supporting Information Section 4 and Table S3 for details on the solubility parameter calculation). Additionally, solvent vapors can effectively alter the interfacial energy at the BCP film interfaces leading to a controlled orientation of BCP structures despite vastly different surface energies of the blocks (in our case, γ = 66 mN/m for PDHS and γ = 34 mN/m for PTMSS).[49] After exposure to the solvent vapors, all the samples produced line/space patterns which are related to the formation of out-of-plane lamellae or in-plane cylinders. The d-spacing were evaluated using FFT from the AFM images at 28.2 nm for PDHS-*b*-PTMSS4, 19.1 nm for PDHS-*b*-PTMSS5, 14.7 nm for PDHS-*b*-PTMSS6, and 11.8 nm for PDHS-*b*-PTMSS7. We tentatively assigned the line-space pattern produced by PDHS-*b*-PTMSS4 to an out-of-plane lamellar structure taking into account the bulk structure resolved by SAXS and the type of self-assembly defects. In particular, edge dislocations and disclinations are clearly apparent on the AFM image [50] and no evidence of characteristic defects related to an in-plane cylindrical structure is apparent (i.e. clusters of out-of-plane perforations related to out-of-plane cylinders or T-junctions at grain boundaries).[51] It is more difficult to draw definitive conclusions for PDHS-*b*-PTMSS5 due to lower quality self-assembly that traps many types of defects, even if a lamellar assembly in the bulk was demonstrated by SAXS. For PDHS-*b*-PTMSS6 and PDHS-*b*-PTMSS7, the formation of in-plane cylinders is coherent with the BCP composition and the SAXS data.

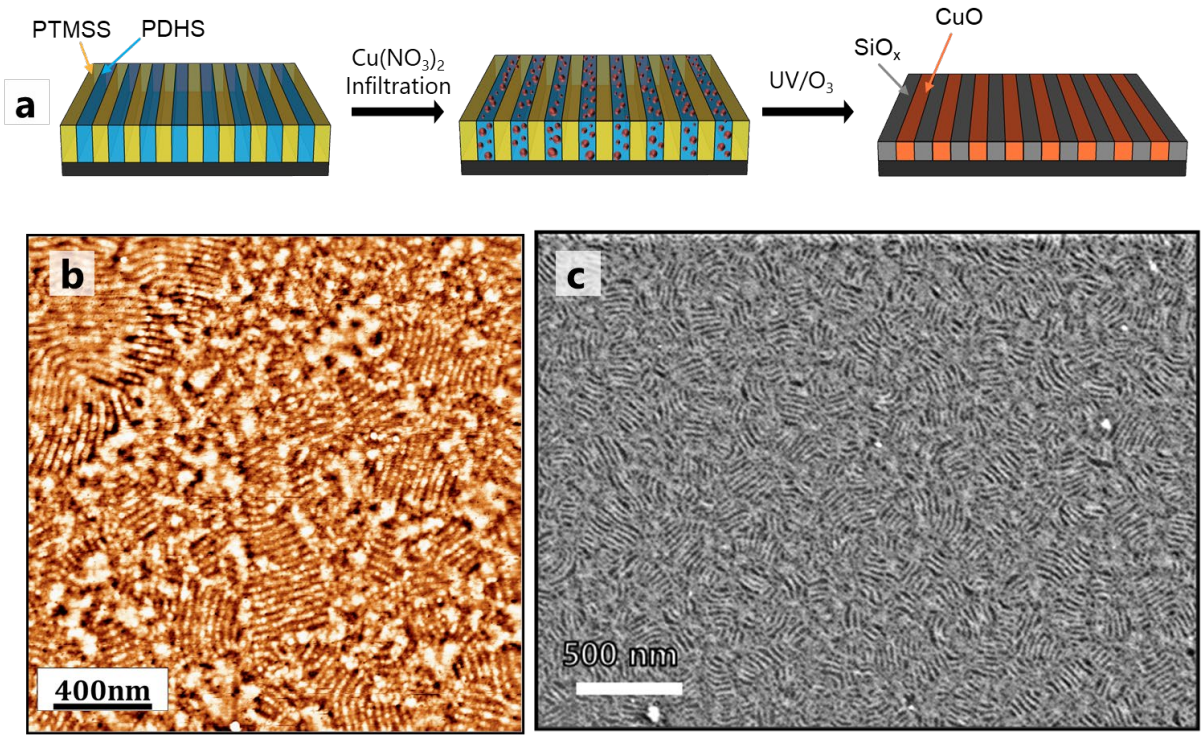


Figure 6. (a) Schematic process for the formation of a dual oxide network with a first infiltration step of $Cu(NO_3)_2$ followed by exposure to UV/O_3. **(b)** AFM height image and **(c)** SEM image of the resulting structure after UV/O_3 exposure.

As a perspective, we also want to emphasize the possibility for this BCP system to be used as a templated nanocomposite (see Figure 6a). The PDHS phase, due to its dense hydrogen-bond providing groups can specifically be infiltrated by metal salts.[52–55] Thus, we opted to infiltrate the PDHS phase with copper nitrate $(CuNO_3)_2$ followed by subsequent oxidation using UV/O_3 irradiation. The aim was to oxidize the copper infiltrated media into copper oxide while the PTMSS domains were transformed into SiO_x. Preliminary results of the proposed SiO_x-CuO nanocomposite structure are presented in Figure 6 b,c (see Supporting Information Section 6 for details). Although the dual network is difficult to fully characterize using top-view imaging techniques such as AFM or SEM, we noticed that the line/space structure is preserved at each step of such treatment (see Figure S10). Additionally, XPS analysis performed on such template

nanocomposite demonstrated the presence of CuO in the infiltrated BCP film with respect to an UV/O_3 exposed PDHS-*b*-PTMSS film (see Figure S11). Even if further investigation is needed to confirm the proper distribution of the CuO and SiO_x domains, such results highlight the potential of BCP systems enabling a dual selective conversion of the BCP domains.

CONCLUSION

Specific styrene-based monomers were synthesized, polymerized and used to design a novel BCP set for the definition of nanometric features as small as 8 nm. Sequential NMP polymerization followed by the deprotection of the diacetoxy derivative in mild conditions yields to a library of well-defined PDHS-*b*-PTMMS BCPs with average molecular weights ranging from 2.1 to 44.5 kg/mol. The morphological behavior of these systems was deciphered using SAXS and demonstrated the ability of this system to form sub-10 nm structures. Additionally, the interaction parameter calculated through temperature resolved SAXS showed a high value of 0.56 at 140°C enabling the use of this system for the definition of high-resolution patterns in thin films. Finally, the vastly different chemical nature of the blocks was shown to drive the formation of template nanocomposite through a dual selective conversion of the BCP domains in oxide derivatives.

SUPPORTING INFORMATION

Polymer synthesis and characterization details; SI sections 1 and 2, Figure S1-S4. Detailed polymer characterizations; Table S1. Normalized GPC traces for all BCPs and precursors; Figure S5. FTIR spectra of PDAS, PDAS-*b*-PTMSS and PDHS-*b*-PTMSS; Figure S6. DSC traces of PDAS-*b*-PTMSS and PDHS-*b*-PTMSS; Figure S7. Details on χ calculation; SI section 3. Solvent-polymer interaction parameter calculation details; SI section 4, Table S3. Self-

assembly in thin-film and film uniformity; SI section 5, Figure S8-S9. Copper oxide infiltration AFM images and XPS analysis; SI section 5, Figure S10-S11.

ACKNOWLEDGMENTS

The authors are sincerely grateful for financial support from the University of Bordeaux. The authors thank Ahmed Bentaleb (CRPP, University of Bordeaux) for SAXS assistance, Melanie Bousquet for the expertise on GPC analysis and The University College London for the temperature-resolved SAXS analysis. The authors also thank the LCPO support staff Aude Manson, Ellena Karnezis, and Gilles Pecastaings for their endless everyday help. This work was performed within the framework of the Equipex ELORPrint- Tec ANR-10-EQPX-28-01 with the help of the French state's Initiative d'Excellence IdEx ANR-10-IDEX-003-02.

REFERENCES

(1) Cummins, C.; Lundy, R.; Walsh, J. J.; Ponsinet, V.; Fleury, G.; Morris, M. A. Enabling Future Nanomanufacturing through Block Copolymer Self-Assembly: A Review. *Nano Today* **2020**, *35*, 100936.

(2) Phillip, W. A.; O'neill, B.; Rodwogin, M.; Hillmyer, M. A.; Cussler, E. L. Self-Assembled Block Copolymer Thin Films as Water Filtration Membranes. *ACS Appl. Mater. Interfaces* **2010**, *2* (3), 847–853.

(3) Orilall, M. C.; Wiesner, U.; Lee, J.; DiSalvo, F. J.; Wiesner, U.; Gruner, S. M.; Baiker, A.; Wiesner, U.; DiSalvo, F. J.; Steiner, U.; Snaith, H. J.; Steiner, U.; Snaith, H. J. Block Copolymer Based Composition and Morphology Control in Nanostructured Hybrid Materials for Energy Conversion and Storage: Solar Cells, Batteries, and Fuel Cells. *Chem. Soc. Rev.* **2011**, *40* (2), 520–535.

(4) Yao, P.; Chen, C.; Shi, S.; Schneider, G. J.; Prather, D. W. Polymer-Based Photonic Crystals. *Opt. InfoBase Conf. Pap.* **2005**, No. 6, 421–425.

(5) Alvarez-Fernandez, A.; Cummins, C.; Saba, M.; Steiner, U.; Fleury, G.; Ponsinet, V.; Guldin, S. Block Copolymer Directed Metamaterials and Metasurfaces for Novel Optical Devices. *Adv. Opt. Mater.* **2021**, *9* (16).

(6) Cummins, C.; Pino, G.; Mantione, D.; Fleury, G. Engineering Block Copolymer Materials for Patterning Ultra-Low Dimensions. *Mol. Syst. Des. Eng.* **2020**, *5* (10), 1642–1657.

(7) Morris, M. A. Directed Self-Assembly of Block Copolymers for Nanocircuitry Fabrication. *Microelectron. Eng.* **2015**, *132*, 207–217.

(8) Black, C. T.; Guarini, K. W.; Ruiz, R.; Sikorski, E. M.; Babich, I. V.; Sandstrom, R. L.;

Zhang, Y. Polymer Self Assembly in Semiconductor Microelectronics. *Tech. Dig. - Int. Electron Devices Meet. IEDM* **2006**, *51* (5), 605–633.

(9) Bates, C. M.; Maher, M. J.; Janes, D. W.; Ellison, C. J.; Willson, C. G. Block Copolymer Lithography. *Macromolecules* **2014**, *47* (1), 2–12.

(10) Brassat, K.; Kool, D.; Nallet, C. G. A.; Lindner, J. K. N. Understanding Film Thickness-Dependent Block Copolymer Self-Assembly by Controlled Polymer Dewetting on Prepatterned Surfaces. *Adv. Mater. Interfaces* **2020**, *7* (1), 1–10.

(11) Cheng, L.-C.; Bai, W.; Fernandez Martin, E.; Tu, K.-H.; Ntetsikas, K.; Liontos, G.; Avgeropoulos, A.; Ross, C. A. Morphology, Directed Self-Assembly and Pattern Transfer from a High Molecular Weight Polystyrene-Block-Poly(Dimethylsiloxane) Block Copolymer Film. *Nanotechnology* **2017**, *28* (14), 145301.

(12) Pang, Y.; Jin, X.; Huang, G.; Wan, L.; Ji, S. Directed Self-Assembly of Styrene-Methyl Acrylate Block Copolymers with Sub-7 Nm Features via Thermal Annealing. *Macromolecules* **2019**, *52* (8), 2987–2994.

(13) Zhang, W.; Huang, M.; Abdullatif, S. Al; Chen, M.; Shao-Horn, Y.; Johnson, J. A. Reduction of (Meth)Acrylate-Based Block Copolymers Provides Access to Self-Assembled Materials with Ultrasmall Domains. *Macromolecules* **2018**, *51* (17), 6757–6763.

(14) Grubbs, R. B. Nitroxide-Mediated Radical Polymerization: Limitations and Versatility. *Polym. Rev.* **2011**, *51* (2), 104–137.

(15) Moad, G.; Rizzardo, E.; Thang, S. H. Radical Addition-Fragmentation Chemistry in Polymer Synthesis. *Polymer (Guildf).* **2008**, *49* (5), 1079–1131.

(16) Zalusky, A. S.; Olayo-Valles, R.; Wolf, J. H.; Hillmyer, M. A. Ordered Nanoporous

Polymers from Polystyrene-Polylactide Block Copolymers. *J. Am. Chem. Soc.* **2002**, *124* (43), 12761–12773.

(17) Sinturel, C.; Bates, F. S.; Hillmyer, M. A. High χ-Low N Block Polymers: How Far Can We Go? *ACS Macro Lett.* **2015**, *4* (9), 1044–1050.

(18) Russell, T. P.; Hjelm, R. P.; Seeger, P. A. Temperature Dependence of the Interaction Parameter of Polystyrene and Poly(Methyl Methacrylate). *Macromolecules* **1990**, *23* (3), 890–893.

(19) Kennemur, J. G.; Yao, L.; Bates, F. S.; Hillmyer, M. A. Sub-5 Nm Domains in Ordered Poly(Cyclohexylethylene)- Block -Poly(Methyl Methacrylate) Block Polymers for Lithography. *Macromolecules* **2014**, *47* (4), 1411–1418.

(20) Park, S.; Dong, H. L.; Xu, J.; Kim, B.; Sung, W. H.; Jeong, U.; Xu, T.; Russell, T. P. Macroscopic 10-Terabit-per-Square-Inch Arrays from Block Copolymers with Lateral Order. *Science (80-.).* **2009**, *323* (5917), 1030–1033.

(21) Kim, S. H.; Misner, M. J.; Yang, L.; Gang, O.; Ocko, B. M.; Russell, T. P. Salt Complexation in Block Copolymer Thin Films. *Macromolecules* **2006**, *39* (24), 8473–8479.

(22) Young, W. S.; Epps, T. H. Salt Doping in PEO-Containing Block Copolymers: Counterion and Concentration Effects. *Macromolecules* **2009**, *42* (7), 2672–2678.

(23) Sweat, D. P.; Kim, M.; Schmitt, A. K.; Perroni, D. V.; Fry, C. G.; Mahanthappa, M. K.; Gopalan, P. Phase Behavior of Poly(4-Hydroxystyrene-Block-Styrene) Synthesized by Living Anionic Polymerization of an Acetal Protected Monomer. *Macromolecules* **2014**, *47* (18), 6302–6310.

(24) Kwak, J.; Kumar Mishra, A.; Lee, J.; Seong Lee, K.; Choi, C.; Maiti, S.; Kim, M.; Kon

Kim, J. Fabrication of Sub-3 Nm Feature Size Based on Block Copolymer Self-Assembly for Next-Generation Nanolithography. *Macromolecules* **2017**, *50*, 6813–6818.

(25) Jung, Y. S.; Ross, C. A. Orientation-Controlled Self-Assembled Nanolithography Using a Polystyrene−Polydimethylsiloxane Block Copolymer. *Nano Lett.* **2007**, *7* (7), 2046–2050.

(26) Luo, Y.; Montarnal, D.; Kim, S.; Shi, W.; Barteau, K. P.; Pester, C. W.; Hustad, P. D.; Christianson, M. D.; Fredrickson, G. H.; Kramer, E. J.; Hawker, C. J. Poly(Dimethylsiloxane- b -Methyl Methacrylate): A Promising Candidate for Sub-10 Nm Patterning. *Macromolecules* **2015**, *48* (11), 3422–3430.

(27) Li, L.; Schulte, L.; Clausen, L. D.; Hansen, K. M.; Jonsson, G. E.; Ndoni, S. Gyroid Nanoporous Membranes with Tunable Permeability. *ACS Nano* **2011**, *5* (10), 7754–7766.

(28) Zhang, S.; Hou, Z.; Gonsalves, K. E. Copolymer Synthesis of Poly(L-Lactide-b-DMS-L-Lactide) via the Ring Opening Polymerization of L-Lactide in the Presence of α,ω-Hydroxylpropyl-Terminated PDMS Macroinitiator. *J. Polym. Sci. Part A Polym. Chem.* **1996**, *34* (13), 2737–2742.

(29) Pitet, L. M.; Wuister, S. F.; Peeters, E.; Kramer, E. J.; Hawker, C. J.; Meijer, E. W. Well-Organized Dense Arrays of Nanodomains in Thin Films of Poly(Dimethylsiloxane)- *b* -Poly(Lactide) Diblock Copolymers. *Macromolecules* **2013**, *46* (20), 8289–8295.

(30) van Genabeek, B.; de Waal, B. F. M.; Gosens, M. M. J.; Pitet, L. M.; Palmans, A. R. A.; Meijer, E. W. Synthesis and Self-Assembly of Discrete Dimethylsiloxane–Lactic Acid Diblock Co-Oligomers: The Dononacontamer and Its Shorter Homologues. *J. Am.*

Chem. Soc. **2016**, *138* (12), 4210–4218.

(31) Jeong, J. W.; Park, W. I.; Kim, M.-J.; Ross, C. A.; Jung, Y. S. Highly Tunable Self-Assembled Nanostructures from a Poly(2-Vinylpyridine- b -Dimethylsiloxane) Block Copolymer. *Nano Lett.* **2011**, *11* (10), 4095–4101.

(32) Durand, W. J.; Blachut, G.; Maher, M. J.; Sirard, S.; Tein, S.; Carlson, M. C.; Asano, Y.; Zhou, S. X.; Lane, A. P.; Bates, C. M.; Ellison, C. J.; Willson, C. G. Design of High-χ Block Copolymers for Lithography. *J. Polym. Sci. Part A Polym. Chem.* **2015**, *53* (2), 344–352.

(33) Takeshima, H.; Satoh, K.; Kamigaito, M. Scalable Synthesis of Bio-Based Functional Styrene: Protected Vinyl Catechol from Caffeic Acid and Controlled Radical and Anionic Polymerizations Thereof. *ACS Sustain. Chem. Eng.* **2018**, *6* (11), 13681–13686.

(34) Lee, J.; Radomkit, S.; Torker, S.; Pozo, J.; Hoveyda, A. H. Mechanism-Based Enhancement of Scope and Enantioselectivity for Reactions Involving a Copper-Substituted Stereogenic Carbon Centre. *Nat. Chem.* **2018**, *10* (1), 99–108.

(35) Legrain, A.; Fleury, G.; Mumtaz, M.; Navarro, C.; Arias-Zapata, J.; Chevalier, X.; Cayrefourcq, I.; Zelsmann, M. Straightforward Integration Flow of a Silicon-Containing Block Copolymer for Line-Space Patterning. *ACS Appl. Mater. Interfaces* **2017**, *9* (49), 43043–43050.

(36) Chevalier, X.; Gomes Correia, C.; Pound-Lana, G.; Bézard, P.; Sérégé, M.; Petit-Etienne, C.; Gay, G.; Cunge, G.; Cabannes-Boué, B.; Nicolet, C.; Navarro, C.; Cayrefourcq, I.; Müller, M.; Hadziioannou, G.; Iliopoulos, I.; Fleury, G.; Zelsmann, M. Lithographically Defined Cross-Linkable Top Coats for Nanomanufacturing with High-χ Block Copolymers. *ACS Appl. Mater. Interfaces* **2021**, *13* (9), 11224–11236.

(37) Jäkle, F. Lewis Acidic Organoboron Polymers. *Coord. Chem. Rev.* **2006**, *250* (9–10), 1107–1121.

(38) Fischer, H. The Persistent Radical Effect in Controlled Radical Polymerizations. *J. Polym. Sci. Part A Polym. Chem.* **1999**, *37* (13), 1885–1901.

(39) Cushen, J. D.; Wan, L.; Pandav, G.; Mitra, I.; Stein, G. E.; Ganesan, V.; Ruiz, R.; Grant Willson, C.; Ellison, C. J.; Willson, C. G.; Ellison, C. J. Ordering Poly(Trimethylsilyl Styrene- Block - D , L -Lactide) Block Copolymers in Thin Films by Solvent Annealing Using a Mixture of Domain-Selective Solvents. *J. Polym. Sci. Part B Polym. Phys.* **2014**, *52* (1), 36–45.

(40) Nakamura, K.; Hatakeyama, T.; Hatakeyama, H. Effect of Substituent Groups on Hydrogen Bonding of Polyhydroxystyrene Derivatives. *Polym. J.* **1983**, *15* (5), 361–366.

(41) Semenov, A. N. Contribution to the Theory of Microphase Layering in Block-Copolymer Melts. *Sov. Phys. JETP* **1985**, *61* (4), 733–742.

(42) Leibler, L. Theory of Microphase Separation in Block Copolymers. *Macromolecules* **1980**, *13* (6), 1602–1617.

(43) Cushen, J. D.; Bates, C. M.; Rausch, E. L.; Dean, L. M.; Zhou, S. X.; Willson, C. G.; Ellison, C. J. Thin Film Self-Assembly of Poly(Trimethylsilylstyrene-b-d, l-Lactide) with Sub-10 Nm Domains. *Macromolecules* **2012**, *45* (21), 8722–8728.

(44) Azuma, K.; Sun, J.; Choo, Y.; Rokhlenko, Y.; Dwyer, J. H.; Schweitzer, B.; Hayakawa, T.; Osuji, C. O.; Gopalan, P. Self-Assembly of an Ultrahigh-χ Block Copolymer with Versatile Etch Selectivity. *Macromolecules* **2018**, *51* (16), 6460–6467.

(45) Paik, M. Y.; Bosworth, J. K.; Smilges, D.-M.; Schwartz, E. L.; Andre, X.; Ober, C. K.

Reversible Morphology Control in Block Copolymer Films via Solvent Vapor Processing: An In Situ GISAXS Study. *Macromolecules* **2010**, *43* (9), 4253–4260.

(46) Bosworth, J. K.; Paik, M. Y.; Ruiz, R.; Schwartz, Ḱ. E. L.; Huang, J. Q.; Ko, A. W.; Smilgies, D.; Black, C. T.; Ober, C. K. Control of Self-Assembly OfLithographically Patternable BlockCopolymer Films. *ACS Nano* **2008**, *2* (7), 1396–1402.

(47) Jarnagin, N. D.; Yeh, W.-M.; Cheng, J.; Peters, A.; Lawson, R. A.; Tolbert, L. M.; Henderson, C. L. PS-b-PHOST as a High χ Block Copolymers for Directed Self Assembly: Optimization of Underlayer and Solvent Anneal Processes. In *Alternative Lithographic Technologies V*; Tong, W. M., Resnick, D. J., Eds.; 2013; Vol. 8680, p 86801X.

(48) Sipos, L.; Som, A.; Faust, R.; Richard, R.; Schwarz, M.; Ranade, S.; Boden, M.; Chan, K. Controlled Delivery of Paclitaxel from Stent Coatings Using Poly(Hydroxystyrene-b-Isobutylene-b-Hydroxystyrene) and Its Acetylated Derivative. *Biomacromolecules* **2005**, *6* (5), 2570–2582.

(49) Sinturel, C.; Vayer, M.; Morris, M.; Hillmyer, M. A. Solvent Vapor Annealing of Block Polymer Thin Films. *Macromolecules* **2013**, *46* (14), 5399–5415.

(50) Kim, S. O.; Kim, B. H.; Kim, K.; Koo, C. M.; Stoykovich, M. P.; Nealey, P. F.; Solak, H. H. Defect Structure in Thin Films of a Lamellar Block Copolymer Self-Assembled on Neutral Homogeneous and Chemically Nanopatterned Surfaces. *Macromolecules* **2006**, *39* (16), 5466–5470.

(51) Horvat, A.; Sevink, G. J. A.; Zvelindovsky, A. V; Krekhov, A.; Tsarkova, L. Specific Features of Defect Structure and Dynamics in the Cylinder Phase of Block Copolymers. *ACS Nano* **2008**, *2* (6), 1143–1152.

(52) Isakova, A.; Topham, P. D.; Sutherland, A. J. Controlled RAFT Polymerization and Zinc Binding Performance of Catechol-Inspired Homopolymers. *Macromolecules* **2014**, *47* (8), 2561–2568.

(53) Ghoshal, T.; Senthamaraikannan, R.; Shaw, M. T.; Holmes, J. D.; Morris, M. A. Fabrication of Ordered, Large Scale, Horizontally-Aligned Si Nanowire Arrays Based on an in Situ Hard Mask Block Copolymer Approach. *Adv. Mater.* **2014**, *26* (8), 1207–1216.

(54) Ghoshal, T.; O'Connell, J.; Sinturel, C.; Andreazza, P.; Holmes, J. D.; Morris, M. A. Solvent Mediated Inclusion of Metal Oxide into Block Copolymer Nanopatterns: Mechanism of Oxide Formation under UV-Ozone Treatment. *Polymer (Guildf).* **2019**, *173* (December 2018), 197–204.

(55) Cummins, C.; Ghoshal, T.; Holmes, J. D.; Morris, M. A. Strategies for Inorganic Incorporation Using Neat Block Copolymer Thin Films for Etch Mask Function and Nanotechnological Application. *Adv. Mater.* **2016**, *28* (27), 5586–5618.